Photodissociation of Linear Carbon Clusters C$_n$ ($n = 4-6$)

Hyeon Choi, Ryan T. Bise, Alexandra A. Hoops, David H. Mordaunt,[†] and Daniel M. Neumark*

Department of Chemistry, University of California, Berkeley, California, 94720, and Chemical Sciences Division, Lawrence Berkeley Laboratory, Berkeley, California 94720

The photodissociation of mass-selected linear carbon clusters (C$_n$, $n = 4-6$) is studied using fast beam photofragment translational spectroscopy. The photofragment yield (PFY) spectra consist of several continua spanning the whole visible and ultraviolet region. The product mass distributions for dissociation of C$_n$ clusters are dominated by C$_3$ and its partner fragment C$_{n-3}$, although some minor channels are also identified for dissociation of C$_4$ and C$_5$ clusters. Translational energy $P(E_T)$ distributions for the C$_3$ + C$_{n-3}$ channel were measured at several photolysis energies. The PFY spectra and $P(E_T)$ distributions indicate that multiphoton dissociation occurs at photon energies below the dissociation threshold and that both single-photon and multiphoton dissociation occur above the threshold. The one-photon components of the $P(E_T)$ distributions can be modeled by phase space theory (PST), suggesting that photoexcitation is followed by internal conversion to the ground state. The PST analysis yields dissociation energies for C$_n \rightarrow$ C$_3$ + C$_{n-3}$ in reasonable agreement with recent Knudsen effusion mass spectrometry measurements.

I. Introduction

Linear carbon clusters have been identified as key reaction intermediates in combustion[1] and the interstellar medium[2−5] leading to the formation of fullerenes[6,7] and soot.[8] These observations have motivated numerous spectroscopic studies, resulting in extensive characterization of the ground and, to a lesser extent, the low-lying electronic states of linear carbon clusters. However, there is less information on the photochemical and thermodynamic properties of carbon clusters. These properties are important for understanding the evolution of carbon cluster geometries with increasing size, namely the transformation from chains to mono- and polycyclic rings and ultimately to fullerenes and other three-dimensional structures. In this article, we address these issues by employing the technique of fast radical beam photofragment translational spectroscopy to study the photodissociation of mass-selected linear carbon clusters. By measuring photofragment yield spectra, product branching ratios, and product translational energy distributions, our experiments probe both the energetics and dissociation dynamics of these clusters.

Much of our understanding of carbon clusters derives from the classic paper of Pitzer and Clementi,[9] who proposed that small neutral clusters are linear molecules with cumulenic bonds. The even-numbered clusters were predicted to be open shell species with $^3\Sigma_g^-$ ground states and high electron affinities, while the odd-numbered clusters were expected to have closed shell $^1\Sigma_g^+$ ground states with considerably lower electron affinities. These predictions have generally been confirmed by experiment and theory. The properties of carbon clusters have been extensively reviewed by Weltner and Van Zee[10] in 1989 and by Van Orden and Saykally[11] in 1998. As is described in the more recent review, a combination of high-resolution gas

phase and matrix spectroscopy, anion photodetachment spectroscopy, and electronic structure calculations has yielded rotational constants and vibrational frequencies for the ground states of linear carbon clusters as large as C$_{13}$. Ion mobility studies provide further information on these and larger clusters,[6,12,13] showing how the geometry of carbon cluster cations and anions evolve from linear to more complex structures as the number of atoms increases. From the perspective of the work to be presented here, the most important results are that the C$_n^-$ anions are linear for $n \leq 9$ and that photodetachment of these anions yields linear neutral carbon clusters.[14−16]

There has also been considerable interest in the excited states of carbon clusters. Electronic transitions in carbon clusters have been proposed as possible candidates for the diffuse interstellar bands.[3,4,17,18] This has motivated Maier and co-workers[19−22] to study the ultraviolet (UV) and visible absorption spectroscopy of mass-selected carbon clusters deposited in a cryogenic matrix, obtaining vibrationally resolved electronic transitions for C$_4$, C$_5$, and C$_6$. Further information on excited electronic states comes from anion photoelectron spectroscopy,[14−16] which reveals states that are optically inaccessible from the neutral ground state, and electronic structure calculations.[23−28] Both experiment and theory indicate a large number of low-lying singlet and triplet states in carbon clusters, an important property from the point of view of the current paper.

Experimental heats of formation ΔH_f for carbon clusters have been previously determined using Knudsen effusion mass spectrometry, in which the relative concentrations of C$_n$ clusters in equilibrium with graphite at high temperature (2000−3000 K) are measured. In 1959, Drowart et al.[29] obtained heats of formation of C$_2$−C$_5$ using this method. However, "third law" extrapolation to ΔH_f at 298 K (or 0 K) requires knowledge of the entropy of carbon clusters, and since some bend frequencies for these species were later found to be very low (i.e., 63 cm^{-1} for C$_3$[30]), the entropy was underestimated in this early measurement.[31,32] More recently, Gingerich and co-workers[33−35] have

* To whom correspondence should be addressed.
† Present address: Coherent Inc., Medical Group, 2400 Condensa Street, Santa Clara, California 95051.
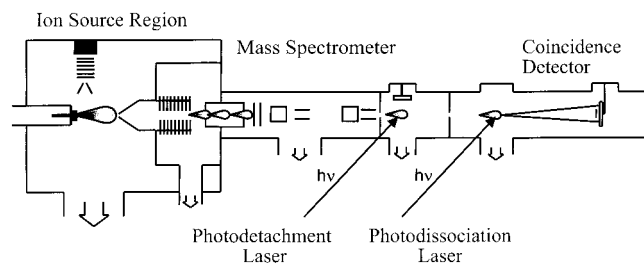
Figure 1. Schematic diagram of the fast beam photofragment translational spectrometer.

performed improved Knudsen measurements. Using the most current spectroscopic data on carbon clusters in their third law extrapolation, they obtained new values of ΔH_f for C_2-C_7 and found significant differences (0.4−0.8 eV) from the original study.

The heats of formation and reaction of carbon clusters have also been calculated in a series of semiempirical and ab initio studies.[23−25,36−41] There are significant differences in the calculated heats of formation, but because of the particular stability of C_3, dissociation of a larger cluster to at least one C_3 fragment is always the lowest energy channel. This is consistent with calculations and experiments for dissociation of carbon cluster anions and cations,[38,42−48] where neutral C_3 elimination is the dominant photodissociation channel.

In this paper, the photodissociation of mass-selected neutral carbon clusters C_4, C_5, and C_6 is investigated for the first time, using fast beam photofragment translational spectroscopy. Neutral carbon clusters are generated by laser photodetachment of the corresponding mass-selected anions. The neutral clusters are then photodissociated and the photofragments detected. The apparatus is described in section II. The experimental results for the photodissociation of C_4, C_5, and C_6 clusters are presented in section III and analyzed in section IV. The results show that multiphoton absorption occurs over a wide range of photon energies, while single-photon dissociation shows statistical behavior near the dissociation threshold. This unusual competition between single-photon multiphoton processes is discussed in section V.

II. Experimental Section

The experimental apparatus shown in Figure 1 has been previously described in detail;[49,50] only a brief description is given here. To generate carbon cluster anions, a pulsed free jet expansion of the gas mixture CO_2:C_2H_2:Ne (mole fraction 1:10:89) passes through a pulsed electric discharge assembly[51] bolted onto the faceplate of the pulsed valve. The core of the free jet passes through a 2 mm diameter skimmer, and the anions are accelerated to 6.5 keV. Mass separation of the ions is accomplished using a collinear Bakker[52] type time-of-flight mass spectrometer. After collimation of the ion beam by a 1.0 mm pinhole, ions are photodetached by an excimer-pumped pulsed dye laser, triggered such that it photodetaches only the ion packet with the mass-to-charge ratio of interest. Thus, a packet of mass-selected neutral radicals is produced. The remaining ions are deflected from the beam. Table 1 lists the photodetachment energy selected for each carbon cluster; this energy was chosen to lie just above the detachment threshold[16,53,54] so that the neutral clusters are produced in their vibrational ground states.

The radicals are collimated by another 1.0 mm pinhole and intersect a second pulsed laser, either an excimer-pumped dye laser or an ArF excimer laser operating at 193 nm. If photodissociation occurs, fragments recoiling out of the parent radical

TABLE 1: Electron Affinities and Detachment Energies Used To Generate Carbon Clusters

	literature electron affinity/eV[a]	detachment energy/eV
$C_4^- \rightarrow C_4 + e^-$	3.882 ± 0.010	4.025
$C_5^- \rightarrow C_5 + e^-$	2.839 ± 0.008	2.877
$C_6^- \rightarrow C_6 + e^-$	4.185 ± 0.006	4.305

[a] As reported by Arnold et al.[15,53]

beam are detected with high sensitivity, *without* an ionization step, using microchannel plate detectors. A beam block immediately in front of the detector stops the remaining neutral beam. Photodissociation occurs under collisionless conditions (10^{-9} Torr), and two types of experiments are performed.

First, the photofragment yield spectrum is obtained by integrating the total fragment flux as a function of photodissociation laser wavelength. Second, at selected fixed photon energies, the dissociation dynamics are investigated by detecting both fragments *in coincidence* from dissociation of a single parent radical. We directly measure three parameters using the time- and position-sensitive detector: the difference in fragment arrival times at the detector, τ, and the distances from the center of the parent neutral beam to each fragment on the detector face, r_1 and r_2. The mass ratio of the photofragments is determined by conservation of linear momentum,

$$\frac{m_1}{m_2} = \frac{r_2}{r_1}\left(1 - \frac{v_0\tau}{L}\right) \qquad (1)$$

where v_0 and L are the parent neutral beam velocity and distance from the photolysis interaction region to the detector. The photofragment translational energy, E_T is also determined from the timing and position information and neutral parent beam energy, E_0,

$$E_T = E_0\frac{m_1m_2}{(m_1+m_2)^2}\frac{[(v_0\tau)^2 + (r_1+r_2)^2]}{L^2} \qquad (2)$$

In the present experimental configuration the translational energy resolution is given by $\Delta E_T/E_T = 2.2\%$.

The flight length to detector (L) can be varied to optimize collection of low or high translational energy fragments. In this paper, $P(E_T)$ distributions for C_4 are reported at 1 m flight length, whereas those for C_5 and C_6 are reported at 2 m flight length. All data shown here are corrected with a "detector acceptance function" (DAF)[49] that accounts for the reduced acceptance of the detector for both high- and low-energy fragments.

III. Results

A. Spectroscopy. Photofragment yield (PFY) spectra were measured over several energy ranges covering the spectral regions 17 980−43 550, 39 990−42 910, and 34 500−48 000 cm^{-1}, for C_4, C_5, and C_6, respectively. A nonzero but unstructured PFY signal was observed over virtually the entire spectral region investigated for each species, generally increasing in intensity with photon energy. C_5 was the only species for which a structured band was observed. This is shown in Figure 2, superimposed on the spectrum obtained by Maier[21] in the same region and assigned to the 2_0^n (symmetric stretch) progression of an optically forbidden (vibronically allowed) electronic transition. The PFY and absorption spectra are not identical; the vibrational features in the PFY spectrum appear to be superimposed on a broader underlying continuum.

Photodissociation of Linear Carbon Clusters

*J. Phys. Chem. A, Vol. 104, No. 10, 2000* **2027**
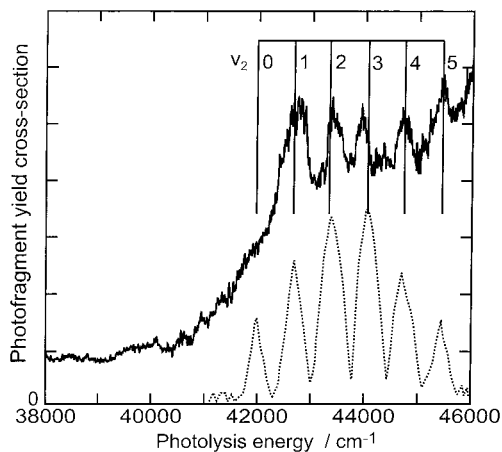
Figure 2. Ultraviolet photofragment yield cross section of C_5 (solid line) and electronic absorption cross-section (dashed line) reproduced from Forney et al.[21] The energy comb plotted above the spectra corresponds to the 2_0^n vibrational progression of the $^1\Sigma_u^+ - \tilde{X}^1\Sigma_g^+$ electronic transition.

Since PFY signal is seen only when dissociation occurs, it is not surprising that the PFY and absorption spectra of carbon clusters are different. What is more intriguing is that any PFY signal is seen over such an extended range of photon enerties. On the basis of the most recent experimental heats of formation by Gingerich and co-workers,[33−35] the bond dissociation energies for C_4, C_5, and C_6 are 5.08 eV (40 970 cm^{-1}), 5.86 eV (47 260 cm^{-1}), and 3.62 eV (29 200 cm^{-1}), respectively. The observation of the PFY signal at energies well below these values implies that multiphoton processes are at play here, in which dissociation occurs only after two or more photons are absorbed. Even the band in Figure 2 begins 0.6 eV below Gingerich's bond dissociation energy, suggesting that it too is from multiphoton absorption. While power dependence studies were attempted at selected photolysis wavelengths, these were generally inconclusive because of the low signal levels observed. Note that similar multiphoton effects were observed in the photodissociation of carbon cluster cations.[44,47]

B. Photofragment Mass Distributions. Analysis of the coincidence time and position data identifies the mass spectrum of the photofragments via eq 1. Quantitative branching ratios between competing photofragment channels are determined by convoluting the raw product mass distribution with the detector acceptance functions[49] for the respective product channels. C_4 primarily dissociates to $C + C_3$, with $C_2 + C_2$ products ranging from 5 to 17% over the photolysis energy range in this study. C_5 dissociates mainly to $C_2 + C_3$; the yield of the minor $C + C_4$ channel is approximately 10% at 5.74 and 5.96 eV and less than 1% at all other incident photolysis energies. C_6 clusters exclusively dissociate to form two C_3 fragments. Overall, production of C_3 is either the dominant or exclusive channel.

C. Translational Energy Distributions. Figures 3−5 report the $P(E_T)$ distributions obtained at selected photolysis energies for C_n dissociation into C_3 and its partner fragment (C_{n-3}) for $n = 4-6$. The low E_T cutoff for each distribution represents the minimum value for which the detector acceptance function is nonzero; at lower values of E_T, no coincident events occur because one or both fragments are blocked by the beam block across the detector face. The larger error bars at low E_T reflect the amplification of the raw data in this energy range by the detector acceptance function.

Three $P(E_T)$ distributions for C_4 at a flight length of 1 m are shown in Figure 3. At a photon energy of 4.59 eV, a signal is seen at a translational energy as high as 2.1 eV. Distributions
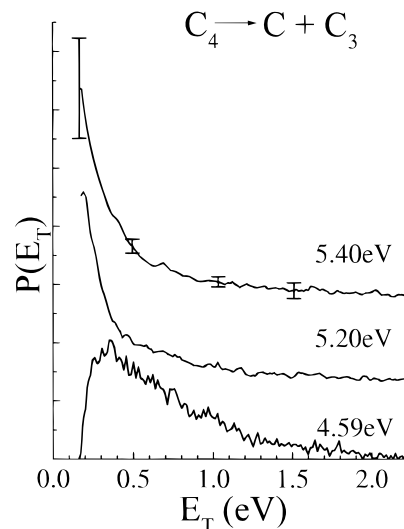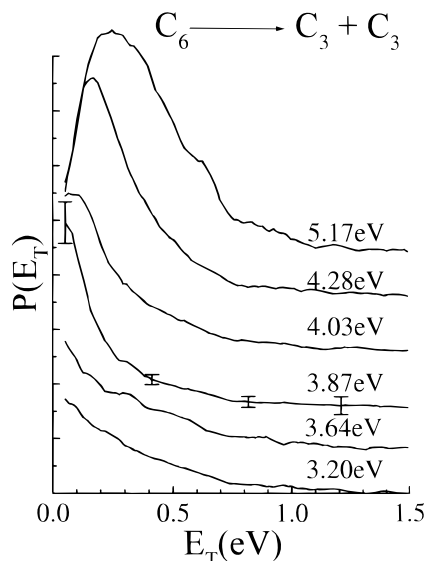

Figure 3. Photofragment translational energy $P(E_T)$ distributions for C_4 dissociation into $C_3 + C$ at 1 m flight length.
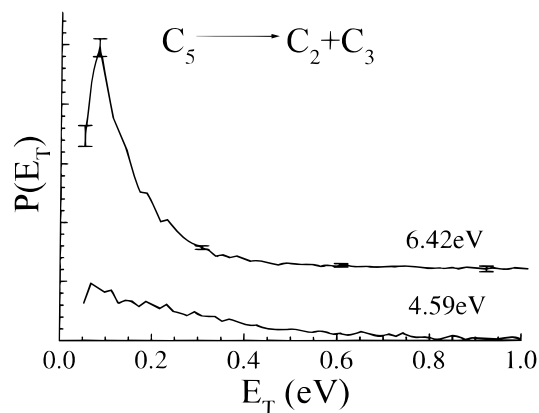
Figure 4. Photofragment translational energy $P(E_T)$ distributions for C_5 dissociation into $C_3 + C_2$ at 2 m flight length.

measured at lower photon energies (not shown) are essentially the same. At 5.20 eV, a new feature appears at $E_T \leq 0.4$ eV, which rises steeply toward low E_T, while the high E_T part of the distribution is essentially unchanged. At 5.40 eV, the new feature broadens somewhat toward higher E_T, whereas the distribution beyond 0.7 eV is very similar to that seen at $h\nu = 4.59$ eV. If the signal at 4.59 eV were due to a one-photon process, then the maximum observed E_T of ∼2.1 eV would imply a bond dissociation energy of 2.5 eV, approximately 2.5 eV below the value of 5.08 eV obtained by Gingerich.[35] Thus, it is reasonable to assume that two-photon processes contribute to the $P(E_T)$ distribution. On the other hand, the sharp feature at low E_T seen for $h\nu \geq 5.20$ eV is consistent with one-photon dissociation and is assigned as such. We thus attribute the entire signal at $h\nu = 4.59$ eV to two-photon dissociation. The signal beyond $E_T = 0.6-0.7$ eV at higher photon energies is also assigned to two-photon dissociation.

Figure 4 shows the $P(E_T)$ distribution for C_5 at two different photon energies, 4.59 and 6.42 eV. The distribution at $h\nu = 4.59$ eV is broad and extends beyond $E_T = 1.0$ eV, whereas an additional sharp peak at $E_T = 0.08$ eV appears at $h\nu = 6.42$ eV. As with C_4, the feature at low E_T is assigned to one-photon dissociation whereas the entire distribution at 4.59 eV and the high E_T component of the distribution at 6.42 eV is assigned to two-photon dissociation. These data were obtained at a flight length of 2 m. The sharp peak at 6.42 eV is not apparent at 1 m flight length, because the translational energy of the photo-

Figure 5. Photofragment translational energy $P(E_T)$ distributions for C_6 dissociation into $C_3 + C_3$ at 2 m flight length.

TABLE 2: Constants for Phase Space Theory Calculations (cm^{-1})

	vibrational frequencies[a]	rotational constant[a]
C_2	1854	1.8198
C_3	1227, 2040, 63[b]	0.4305

[a] Most of vibrational frequencies from ref 19. [b] Degenerate vibrational modes.

fragments is so low that they are largely blocked by the beam block at the shorter flight length.

Figure 5 shows several $P(E_T)$ distributions for C_6 dissociation measured at a flight length of 2 m. The distributions at 3.20 and 3.64 eV are quite similar, extending to $E_T = 1.3$ eV. At $h\nu = 3.87$ eV, a sharp feature at $E_T \leq 0.3$ eV appears, and this feature shifts toward higher E_T and broadens as the photon energy is raised, similar to the trends seen for the sharp peak in C_4 photodissociation. Just as for the smaller clusters, the feature at low E_T is assigned to one-photon dissociation while the high E_T signal is attributed to two-photon dissociation. At photon energies where both processes occur, the delineation between the one- and two-photon components is not as clear as for the smaller clusters. However, if the two-photon component is assumed to be independent of photon energy, as it appears to be for C_4 and C_5, then one can determine the two contributions using the $P(E_T)$ distributions at $h\nu = 3.64$ eV, where no one-photon signal is apparent.

IV. Analysis

Our $P(E_T)$ distributions show contributions from single-photon and multiphoton dissociation. Both the form and energy dependence of one-photon and multiphoton distributions are of importance in deducing the underlying dynamics. The one-photon distribution peaks at low E_T and shows a weak but noticeable dependence on the photon energy, shifting toward higher E_T as the photon energy is raised above the threshold for the one-photon process. The multiphoton component of the $P(E_T)$ distributions also is maximal at low E_T and appears to be independent of the photon energy. Translational energy distributions that peak at low E_T and show a weak dependence on total energy are often a signature of statistical dissociation on a potential energy surface with no exit barrier. Such a distribution could result if photoexcitation is followed by internal

conversion to the ground-state surface, and the resulting microcanonical ensemble lives long enough for the available energy to be randomized among the vibrational modes of the molecule. To test this possibility, both the one-photon and multiphoton distributions are calculated using phase space theory (PST),[55] a reasonable statistical model to apply in the case of barrierless dissociation.

In PST, all product states allowed by conservation of energy and angular momentum are assumed equally probable. Conservation of angular momentum requires that

$$\mathbf{J_{AB}} = \mathbf{J_A} + \mathbf{J_B} + \mathbf{L} \tag{3}$$

where $\mathbf{J_{AB}}$, $\mathbf{J_A}$, and $\mathbf{J_B}$ are the total angular momenta of parent (AB) and fragments (A and B), and $\mathbf{L}$ is the relative orbital angular momentum of the photofragments. Energy conservation and dynamical constraints (e.g., the centrifugal barrier) impose an upper limit l_{max} on L assuming a $V(r) = -C_0/r^6$ potential[56]

$$L(L + 1)h^2 \leq 24\pi^2 \mu C_0^{1/3}(E_T/2)^{2/3} \tag{4}$$

where μ is the reduced mass of the photofragments.

The resulting translational energy distributions are calculated using[56]

$$P^{PST}(E_T) = \int_0^{nh\nu - E_T - D_0} \sum_{J_A}^{J_A^{max}} \sum_{J_B}^{J_B^{max}} \rho_V(E_V) \, N_R(J_A, J_B) \, \delta(nh\nu - E_T - E_V - E_R - D_0) \, dE_V \tag{5}$$

Here D_0 and $nh\nu$ (we assume $n = 2$ in modeling the multiphoton component) are dissociation energies of C_n and total energy, respectively. The energies for product vibrational (V) and rotational (R) degrees of freedom are denoted by $E_{V,R}$ and the density of state for the vibrational (V) degree of freedom is denoted by ρ_V. In eq 5, $N_R(J_A, J_B)$ represents the number of possible combinations of $\mathbf{J_A}$ and $\mathbf{J_B}$ that satisfy eqs 3 and 4, weighted by a Boltzmann distribution for J_{AB} (see eq 9 below).

Using energy conservation the maximum rotational angular momenta of the fragments can be obtained:

$$J_A^{max} = [(nh\nu - D_0 - E_T - E_V)/B_A + 0.25]^{1/2} - 0.5 \tag{6}$$

$$J_B^{max} = [(nh\nu - D_0 - E_T - E_R^A - E_V)/B_B + 0.25]^{1/2} - 0.5 \tag{7}$$

$$E_R^A = B_A J_A(J_A + 1) \tag{8}$$

J_A^{max} and J_B^{max} are the maximum angular momenta of fragment A with E_T and E_V specified and of fragment B with E_T, E_V, and E_R^A (rotational energy of fragment A with $\mathbf{J_A}$) specified, while B_A and B_B are the rotational constants of fragments A and B, given in Table 2.

The vibrational density of states, $\rho_V(E_V)$, is calculated for all energetically allowed vibrational levels within the harmonic oscillator approximation, using the Beyer−Swinehart algorithm;[57] product vibrational frequencies are listed in Table 2. $N_R(J_A, J_B)$, is calculated using:[56]

$$N_R(J_A, J_B) = \sum_{J_{AB}} \sum_{J = |J_{AB} - J_A|}^{J_{AB} + J_A} N_S(J_B, J) \, P_{Bolt}(J_{AB}) \tag{9}$$

for which

Photodissociation of Linear Carbon Clusters

J. Phys. Chem. A, Vol. 104, No. 10, 2000 **2029**

$$N_S(J_B, J) = 0 \qquad l_{max} \le |J_B - J|$$
$$= l_{max} - |J_B - J| + 1 \qquad |J_B - J| < l_{max} < J_B + J$$
$$= J_B + J - |J_B - J| + 1 \qquad l_{max} \ge J_B + J$$
$$P_{Bolt}(J_{AB}) = g_{J_{AB}} \exp(-B_{AB} J_{AB}(J_{AB} + 1)/k_B T)/Q_{J_{AB}}$$

Here $N_S(J_B, J)$ is the number of product rotational states with J_A, J_B, and J_{AB} specified, T is the rotational temperature of AB, and P_{Bolt} is the population of state J_{AB}. The rotational temperature of our beam is estimated to be 50 K. At selected energies, we found essentially no difference in $P^{PST}(E_T)$ distributions calculated at $T = 50$ K or $T = 0$ K ($J_{AB} = 0$), so the latter condition was assumed for all calculations reported below.

To compare the PST distributions with experiment, the calculated distributions were convoluted with a Monte Carlo simulation program[49,50] that simulates all the apparatus parameters, including the ion/radical beam angular and velocity distribution, the finite interaction volumes, the resolution of the time and position detector, the size of the beam block, and the area of the two-particle detector. It became apparent by inspection that the multiphoton component of the $P(E_T)$ distributions could *not* be fit by PST. The calculated distributions extended to much higher translational energies than the experimental distributions, even assuming only two photons were absorbed. Therefore, since this component appears independent of the photon energy, we simply added the one-photon distribution calculated via PST at a particular photon energy to the experimental multiphoton distribution obtained at a photon energy where no one-photon dissociation was observed; this hybrid distribution could then be directly compared to the experimental distribution.

To find the best one-photon PST distribution that can properly describe the experimental data, C_0 and D_0 in eqs 4 and 5 are used as variable parameters. Varying C_0 from 10 to 100 eV·Å[6] yielded only small changes in the calculated distributions. The value of 10 eV·Å,[6] a reasonable number for species in this size range,[58] was chosen for all calculations. The calculated distributions were more sensitive to the dissociation energy (D_0), for which optimal values are given in Table 3 along with those obtained previously by Gingerich.[33-35] When error bars for both measurements are considered, our value of D_0 for C_4 lies barely below that obtained by Gingerich, while the values for C_5 and C_6 agree.

Calculated and experimental $P(E_T)$ distributions are compared in Figures 6, 7 (upper panel), and 8 for dissociation of C_4, C_5, and C_6, respectively. Each figure shows the assumed multiphoton distribution, the Monte Carlo convoluted PST distribution, and the sum of the two. We find excellent agreement for the C_4 and C_5 distributions, and for C_6 at the two lower photolysis energies shown in Figure 8.

The agreement between experimental and simulated $P(E_T)$ distributions using dissociation energies similar to those obtained by Gingerich[34,35] supports our statistical hypothesis for the one-photon component of the distributions, at least near the threshold

TABLE 3: Measured Bond Dissociation Energies for Carbon Clusters

|	bond dissociation energies/eV	
photofragmentation channel	PST calculation, this work	Gingerich et al.[34,35]
$C_4 \rightarrow C + C_3$	4.71 ± 0.15	5.08 ± 0.21
$C_5 \rightarrow C_2 + C_3$	5.96 ± 0.15	5.88 ± 0.23
$C_6 \rightarrow C_3 + C_3$	3.32 ± 0.20	3.63 ± 0.27
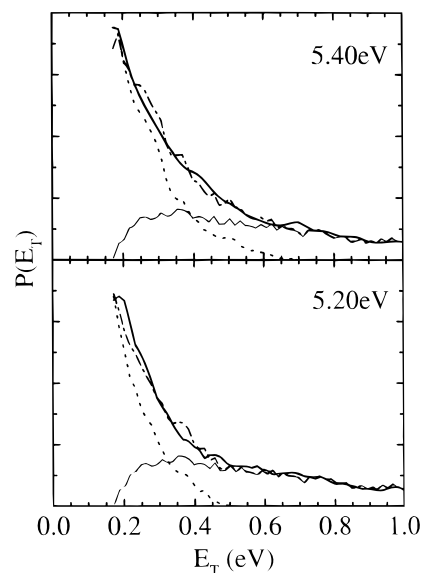
Figure 6. Comparison of experimental $P(E_T)$ distributions to calculated PST distributions for unimolecular dissociation of the C_4 into C_3 + C products. The assumed multiphoton distribution (thin solid line), the Monte Carlo convoluted PST distribution (dotted line), and the sum of two (dash−dotted line) are plotted with the experimental $P(E_T)$ distribution (thick solid line).
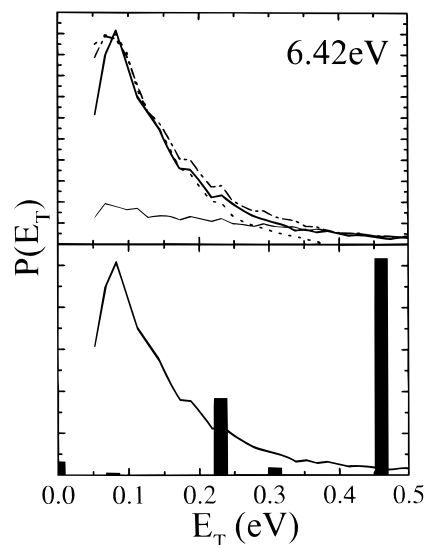
Figure 7. Comparison of experimental $P(E_T)$ distribution for unimolecular dissociation of C_5 into C_3 + C_2 products at 6.42 eV to calculated PST distribution (upper panel) and Franck−Condon (FC) vibrational distribution (lower panel). In the upper panel, the assumed multiphoton distribution (thin solid line), the Monte Carlo convoluted PST distribution (dotted line), and the sum of two (dash−dotted line) are plotted with the experimental $P(E_T)$ distribution (thick solid line). In the lower panel, the results of the FC model are histogrammed since only widely spaced C_2 and C_3 stretching vibrational levels are populated.

for one-photon dissociation. However, for C_6 dissociation at $h\nu \ge 4.28$ eV, the one-photon component of the experimental $P(E_T)$ distributions clearly peaks at nonzero E_T, and this is not reproduced by the PST distribution, as shown in the upper panel of Figure 8. This disagreement may reflect ground-state dissociation that is too fast for a statistical model to be applicable. It is also possible that the dissociation dynamics are fundamentally different for C_6 at these higher energies, involving, for example, a potential energy surface with a significant barrier.

Although our results are generally consistent with statistical dissociation on the ground state, one might ask if there are
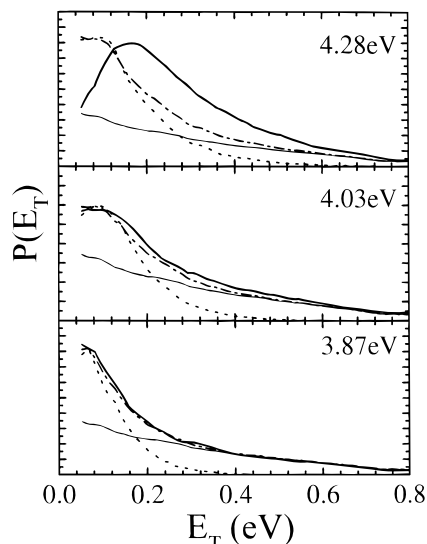
Figure 8. Comparison of experimental $P(E_T)$ distributions to calculated PST distributions for unimolecular dissociation of the C_6 into $C_3 + C_3$ products. The assumed multiphoton distribution (thin solid line), the Monte Carlo convoluted PST distribution (dotted line), and the sum of two (dash−dotted line) are plotted with the experimental $P(E_T)$ distribution (thick solid line).

excited-state dissociation mechanisms that would produce similar translational energy distributions peaking at low E_T and showing little variation with photon energy. One simple mechanism of this type is the Franck−Condon model,[59] applicable for rapid dissociation on a repulsive excited-state surface, in which the product vibrational distribution is given by a Franck−Condon projection of the reactant geometry onto the product vibrational states. Results are given in the lower panel of Figure 7 for photodissociation of C_5; the primary Franck−Condon activity is in the C_2 stretch. Clearly, this distribution peaks at higher E_T than the experimental and statistical distributions (assuming the same bond dissociation energy). Note that any relaxation of the Franck−Condon vibrational distribution due to dynamics on the excited-state surface is likely to increase the fraction of available energy appearing as product translation, resulting in even poorer agreement with the experimental and statistical distributions.

V. Discussion

The principal results from the photodissociation of linear carbon clusters are summarized as follows:

(i) The photofragment yield cross sections consist of several continua spanning the whole visible and ultraviolet region.

(ii) Product branching ratios for dissociation of mass-selected carbon C_n clusters are dominated by the $C_3 + C_{n-3}$ channel, although some minor channels are also identified for dissociation of C_4 and C_5 clusters.

(iii) Analysis of the photofragment translational energy $P(E_T)$ distributions above the dissociation threshold comprise single-photon and multiphoton contributions, confirming that these two processes compete.

(iv) Single-photon dissociation near the threshold results in $P(E_T)$ distributions that are consistent with calculated PST distributions; i.e., the product state distributions are statistical. This implies that dissociation occurs on the ground-state potential energy surface and that no barriers are present along the dissociation coordinates.

(v) Multiphoton dissociation results in structureless $P(E_T)$ distributions extending to high E_T, which show no change with increasing photon energy.

In this section some of these aspects of the dissociation dynamics are considered in more detail. The agreement between the single photon distributions and PST predictions indicates that there are no significant barriers present along the minimum energy pathway from the ground-state minimum to dissociation asymptotes. Linear C_4 and C_6 have $\tilde{X}\ ^3\Sigma_g^-$ ground states, while C_5 has a $\tilde{X}\ ^1\Sigma_g^+$ ground state. For C_4 and C_5, the ground-state surfaces adiabatically correlate with ground-state products, i.e., $C(^3P) + C_3(X\ ^1\Sigma_g^+)$ and $C_2(X\ ^1\Sigma_g^+) + C_3(\tilde{X}\ ^1\Sigma_g^+)$, so the absence of an exit barrier for ground-state dissociation is not unexpected. However, the ground state of C_6 correlates to the $C_3(\tilde{X}\ ^1\Sigma_g^+) + C_3(\tilde{a}\ ^3\Pi_u)$ excited-state asymptote, whereas dissociation to the lowest energy $C_3(\tilde{X}\ ^1\Sigma_g^+) + C_3(\tilde{X}\ ^1\Sigma_g^+)$ channel is spin-forbidden. The $C_3(\tilde{a}\ ^3\Pi_u)$ state lies 2.12 eV above the $C_3(\tilde{X}\ ^1\Sigma_g^+)$ state, and it is extremely unlikely that the one-photon distributions in Figure 5 are due to the triplet product channel since this would imply a bond dissociation energy of 1.2 eV for C_6.

The $C_3(\tilde{X}\ ^1\Sigma_g^+) + C_3(\tilde{X}\ ^1\Sigma_g^+)$ channel can only result from intersystem crossing (ISC) to a low-lying singlet surface. The $\tilde{b}\ ^1\Sigma_g^+$ state is the lowest singlet state that correlates adiabatically to this channel. Liang et al.[60] and Hanrath et al.[61] calculate the $\tilde{b}\ ^1\Sigma_g^+$ to lie only 0.16 and 0.27 eV, respectively, above the $\tilde{X}\ ^3\Sigma_g^-$ ground state, while the C_6^- photoelectron spectrum[16] indicates this splitting is around 0.25 eV. In any case, there will be a curve-crossing between the two states below the dissociation energy. In addition, at the excitation energies in Figure 6 (3.2 eV and higher), the density of vibrational levels in the two C_6 electronic states is quite high ($>10^{10}/cm^{-1}$), so that each triplet vibrational level will be nearly degenerate with a singlet level. Since even a small spin−orbit interaction can result in strong mixing of nearly degenerate singlet and triplet levels, ISC between the two states should be reasonably rapid, consistent with our $P(E_T)$ distributions for C_6 dissociation. We point out that an equal mass (i.e., $C_3 + C_3$) channel has the most favorable mass combination for coincidence detection. As a result, fragments with E_T as low as 0.050 eV can be detected in coincidence (see Figure 5), so we would be particularly sensitive to an exit barrier for dissociation of C_6.

The facile multiphoton absorption and dissociation observed for these carbon clusters is similar to that seen in carbon cluster cations (C_n^+), as discussed by Sowa et al.[47] In both cases, this phenomenon is likely related to a rather large number of low-lying electronic states for these species. For example, nine electronically excited states, three of which are singlets, are calculated to lie within 3 eV of the ground state in C_5,[28] and even more low-lying states are calculated for C_6.[61] The experimental photoelectron spectra of C_4^-, C_5^-, and C_6^- all show transitions to numerous low-lying electronic states of the neutral.[14,16] While transitions to many of these excited states from the neutral ground states are optically forbidden, Maier[21] does observe several weak transitions in his matrix absorption spectra of neutral carbon clusters that are assigned to forbidden transitions allowed by vibronic coupling, including the band that we also observe in Figure 2. Our observation of a finite and essentially continuous photofragment yield across much of the visible and ultraviolet suggests that a combination of vibronic and possibly spin−orbit coupling results in a small but finite oscillator strength for absorption of one photon over a broad energy range, followed by absorption of a second photon and dissociation.

There are two limits for the mechanism of subsequent photon absorption. One is that the excited state generated by the first photon absorbs a second photon before undergoing any signifi-

Photodissociation of Linear Carbon Clusters

J. Phys. Chem. A, Vol. 104, No. 10, 2000 **2031**

cant relaxation. This results in a state with electronic energy $2h\nu$, which could either dissociate or absorb another photon; we did observe a nonzero PFY signal at photon energies that would require three-photon absorption to dissociate. Given that there appears to be a resonant (if weak) transition available from the ground state over a wide energy range, it would not be too surprising if a similar condition held for the one-photon excited state.

Alternatively, absorption of each photon could be followed by internal conversion back to the ground state prior to absorption of the next photon. Thus, electronic energy is converted into vibrational energy on the ground-state surface before a second photon is absorbed, and this process continues until $nh\nu > D_0$. This model is more consistent with the single-photon dynamics seen here; if IC to the ground state dominates just above the dissociation threshold, then it is likely to dominate below the threshold too. It is similar to the mechanism we have proposed for resonant multiphoton detachment of carbon cluster anions.[62] However, as discussed in section IV, the multiphoton $P(E_T)$ distributions appear to be nonstatistical. Thus, it is not clear if absorption of the last photon would be followed by internal conversion and then dissociation on the ground state or by excited-state dissociation. Nonstatistical dissociation on the ground state could occur if the total energy is so high that dissociation is faster than energy randomization; this situation could certainly arise in the case of multiphoton absorption, yielding total energies well in excess of the bond dissociation energy.

VI. Conclusions

We have employed the technique of fast radical beam photofragment translational spectroscopy to study the photo-dissociation of mass-selected linear carbon clusters C_n ($n = 4-6$) and measured the photofragment yield cross-section, product branching ratios, and $P(E_T)$ distributions. The results and analysis indicate somewhat surprising photophysics for these clusters, as they appear to absorb light and dissociate over a wide range of visible and ultraviolet wavelengths. Multiphoton absorption and dissociation occurs at photon energies below the dissociation threshold, while both single-photon and multiphoton dissociation occur above threshold. The single-photon mechanism appears to involve rapid internal conversion to the ground state followed by dissociation primarily to the lowest energy $C_3 + C_{n-3}$ channel.

Our results, particularly the observation of dissociation at photon energies well below the bond dissociation energy, suggest an unprecedented level of electronic and vibrational-state mixing for species in this size regime. We attribute this to the large number of low-lying electronic states in carbon clusters, along with the high density of vibrational levels arising from the low-frequency bends in these species. It would be of considerable interest to attempt to track the energy flow after electronic excitation in these clusters in order to assess the role of the low-lying electronic states. The dominance of ground-state dissociation in our experiments indicates that nanosecond lasers are too slow for doing this, but femtosecond pump–probe measurements based on either ionization or photoelectron detection may provide significantly more insight into the detailed intramolecular dynamics of these species.

References and Notes

(1) Gerhardt, P.; Loffler, S.; Homann, K. H. *Chem. Phys. Lett.* **1987**, *137*, 306.

(2) Goebel, J. H.; Bregman, J. D.; Strecker, D. W.; Witteborn, F. C.; Erckson, E. F. *Astrophys. J.* **1978**, *222*, L129.

(3) Hinkle, K. H.; Keady, J. J.; Bernath, P. F. *Science* **1988**, *241*, 1319.

(4) Bernath, P. F.; Hinkle, K. H.; Keady, J. J. *Science* **1989**, *244*, 562.

(5) Kroto, H. W.; Heath, J. R.; O'Brien, S. C.; Curl, R. F.; Smalley, R. E. *Astrophys. J.* **1987**, *314*, 352.

(6) von Helden, G.; Hsu, M.-T.; Gotts, N.; Bowers, M. T. *J. Phys. Chem.* **1993**, *97*, 8182.

(7) Alexandrov, A. L.; Schweigert, V. A. *Chem. Phys. Lett.* **1996**, *263*, 551.

(8) Ebert, L. B. *Science* **1990**, *247*, 1468.

(9) Pitzer, K. S.; Clementi, E. *J. Am. Chem. Soc.* **1959**, *81*, 4477.

(10) Weltner, W.; Van Zee, R. *Chem. Rev.* **1989**, *89*, 1713–1747.

(11) Van Orden, A.; Saykally, R. J. *Chem. Rev.* **1998**, *98*, 2313–2357.

(12) von Helden, G.; Hsu, M. T.; Gotts, N. G.; Kemper, P. R.; Bowers, M. T. *Chem. Phys. Lett.* **1993**, *204*, 15.

(13) Bowers, M. T.; Kemper, P. R.; von Helden, G.; van Koppen, P. *Science* **1993**, *260*, 1446.

(14) Yang, S. H.; Taylor, K. J.; Craycraft, M. J.; Conceicao, J.; Pettiette, C. L.; Cheshnovsky, O.; Smalley, R. E. *Chem. Phys. Lett.* **1988**, *144*, 431.

(15) Arnold, D. W.; Bradforth, S. E.; Kitsopoulos, T. N.; Neumark, D. M. *J. Chem. Phys.* **1991**, *95*, 8753–8764.

(16) Xu, C.; Burton, G. R.; Taylor, T. R.; Neumark, D. M. *J. Chem. Phys.* **1997**, *107*, 3428–3436.

(17) Douglas, A. E. *Nature* **1977**, *269*, 130.

(18) Fulara, J.; Lessen, D.; Freivogel, P.; Maier, J. P. *Nature* **1993**, *366*, 439.

(19) Freivogel, P.; Grutter, M.; Forney, D.; Maier, J. P. *Chem. Phys. Lett.* **1996**, *249*, 191.

(20) Freivogel, P.; Fulara, J.; Jakoi, M.; Forney, D.; Maier, J. P. *J. Chem. Phys.* **1995**, *103*, 54.

(21) Forney, D.; Freivogel, P.; Grutter, M.; Maier, J. P. *J. Chem. Phys.* **1996**, *104*, 4954.

(22) Forney, D.; Fulara, J.; Freivogel, P.; Jakoi, M.; Lessen, D.; Maier, J. P. *J. Chem. Phys.* **1995**, *103*, 48.

(23) Martin, J. M. L.; Francois, J. P.; Gijbels, R. *J. Chem. Phys.* **1990**, *93*, 8850.

(24) Martin, J. M. L.; Francois, J. P.; Gijbels, R. *J. Chem. Phys.* **1991**, *94*, 3753.

(25) Martin, J. M. L.; Francois, J. P.; Gijbels, R. *J. Comput. Chem.* **1991**, *12*, 52.

(26) Parasuk, V.; Almlof, J. *J. Chem. Phys.* **1989**, *91*, 1137.

(27) Parasuk, V.; Almlof, J. *J. Chem. Phys.* **1991**, *94*, 8172.

(28) Kolbuszewski, M. *J. Chem. Phys.* **1995**, *102*, 3679.

(29) Drowart, J.; Burns, R. P.; DeMarie, G.; Inghram, M. G. *J. Chem. Phys.* **1959**, *31*, 1131.

(30) Gausset, L.; Herzberg, G.; Lagerquist, A.; Rosen, B. *Discuss. Faraday Soc.* **1963**, *35*, 1131.

(31) Strauss, H. L.; Thiele, E. *J. Chem. Phys.* **1967**, *46*, 2473.

(32) Chase, M. W. Jr.; Davies, C. A.; Downey, J. R. Jr.; Fruip, D. J.; McDonald, R. A.; Syverud, A. N. *JANAF Thermochemical Tables*, 3rd ed.; *J. Chem. Phys. Ref. Data 1985, 14,* Suppl. No. 1.

(33) Gingerich, K. A. *Chem. Phys. Lett.* **1992**, *196*, 245.

(34) Gingerich, K. A.; Finkbeiner, H. C.; Schmude, W., Jr. *Chem. Phys. Lett.* **1993**, *207*, 23.

(35) Gingerich, K. A.; Finkbeiner, H. C.; Schmude, W., Jr. *J. Am. Chem. Soc.* **1994**, *116*, 3884.

(36) Martin, J. M. L.; Francois, J. P.; Gijbels, R. *J. Chem. Phys.* **1989**, *90*, 3403.

(37) Raghavachari, K.; Whiteside, R. A.; Pople, J. A. *J. Chem. Phys.* **1986**, *85*, 6623.

(38) Raghavachari, K.; Binkley, J. S. *J. Chem. Phys.* **1987**, *87*, 2191.

(39) Watts, J. D.; Gauss, J.; Stanton, J. F.; Bartlett, R. J. *J. Chem. Phys.* **1992**, *97*, 8372.

(40) Szczepanski, J.; Ekern, S.; Vala, M. *J. Phys. Chem.* **1997**, *101*, 1841.

(41) Slanina, Z. *Chem. Phys. Lett.* **1987**.

(42) Deluca, M. J.; Johnson, M. A. *Chem. Phys. Lett.* **1988**, *152*, 67.

(43) Pozniak, B.; Dunbar, R. C. *Int. J. Mass Spec. Ion Processes* **1994**, *133*, 97.

(44) Geusic, M. E.; McIlrath, T. J.; Jarrold, M. F.; Bloomfield, L. A.; Freeman, R. R.; Brown, W. L. *J. Chem. Phys* **1986**, *84*, 2421.

(45) Radi, P. P.; Bunn, T.; Kemper, P. R.; Molchan, M.; Bower, M. T. *J. Chem. Phys.* **1988**, *88*, 2809.

(46) Schelimov, K. B.; Hunter, J. M.; Jarrold, M. F. *Int. J. Mass Spectrom. Ion Processes* **1994**, *138*, 17.

(47) Sowa, M. B.; Hintz, P. A.; Anderson, S. L. *J. Chem. Phys.* **1991**, *95*, 4719.

(48) Sowa-Resat, M. B.; Hintz, P. A.; Anderson, S. L. *J. Phys. Chem.* **1995**, *99*, 10736.

(49) Continetti, R. E.; Cyr, D. R.; Osborn, D. L.; Leahy, D. J.; Neumark, D. M. *J. Chem. Phys.* **1993**, *99*, 2616.

(50) Continetti, R. E.; Cyr, D. R.; Metz, R. B.; Neumark, D. M. *Chem. Phys. Lett.* **1991**, *182*, 406−411.

(51) Osborn, D. L.; Leahy, D. J.; Cyr, D. R.; Neumark, D. M. *J. Chem. Phys.* **1996**, *104*, 5026.

(52) Bakker, J. M. B. *J. Phys. E* **1973**, *6*, 785.

(53) Kitsopoulos, T. N.; Chick, C. J.; Zhao, Y.; Neumark, D. M. *J. Chem. Phys.* **1991**, *95*, 5479−5481.

(54) Arnold, C. C.; Zhao, Y. X.; Kitsopoulos, T. N.; Neumark, D. M. *J. Chem. Phys.* **1992**, *97*, 6121−6135.

(55) Pechukas, P.; Light, J. C. *J. Chem. Phys.* **1965**, *42*, 3281.

(56) Pechukas, P.; Light, J. C.; Rankin, C. *J. Chem. Phys.* **1966**, *44*, 794.

(57) Robinson, P. J.; Holbrook, K. A. *Unimolecular reactions*; Wiley-Interscience: New York, 1972.

(58) Aquilanti, V.; Cappellitti, D.; Lorent, V.; Luzzatti, E.; Pirani, F. *J. Phys. Chem.* **1993**, *97*, 2063−2071.

(59) Schinke, R. *Photodissociation dynamics*; Cambridge University Press: New York, 1993.

(60) Liang, C.; Schaeffer, H. F., III *Chem. Phys. Lett.* **1990**, *169*, 150.

(61) Hanrath, M.; Peyerimhoff, S. D.; Grein, F. *Chem. Phys.* **1999**, *249*, 121−128.

(62) Zhao, Y.; de Beer, E.; Xu, C.; Taylor, T.; Neumark, D. M. *J. Chem. Phys* **1996**, *105*, 4905.